

Low temperature in-situ preparation of reduced graphene oxide/ZnO nanocomposites for highly sensitive photodetectors

Sisi Liu¹ · Bo Li¹ · Hao Kan¹ · Huan Liu¹ · Bing Xie¹ · Xiao Zhu¹ · Youyou Hu¹ · Shenglin Jiang¹

Received: 13 November 2016 / Accepted: 28 February 2017 / Published online: 9 March 2017
© Springer Science+Business Media New York 2017

Abstract Unlike traditional approach to improve photoreponse performance of ZnO-based optoelectronic devices, a ultra-low temperature solvothermal process was utilized to prepare reduced graphene oxide (rGO)/ZnO nanocomposites, which realized non-surfactant in-situ preparation of rGO/ZnO nanocomposites with the reduction of graphene oxide (GO) at the low temperature process (<170 °C). The effect of annealing process on the microstructure and photoelectronic properties of rGO/ZnO nanocomposites and pure ZnO was investigated. The diameter of as-synthesized ZnO nanocrystal in GO/ZnO precursor was about 6.5 nm. The Fourier transform infrared (FTIR) and Raman spectrum results showed that graphene oxide in the precursor has been reduced to rGO. When annealing at a mild temperature below 170 °C, the optimum photocurrent of rGO/ZnO nanocomposites was about 4.5 times compared to pure ZnO, and the corresponding detectivity reached 6.39×10^{10} Jones. The advantage of the low temperature in-situ technic provides an avenue to fabricate high-performance and low-cost optoelectronic devices.

1 Introduction

Reduced graphene oxide (rGO) is a new class of carbon family with unique two dimensional conjugated structure,

possessing superior mobility of charge carriers at room temperature ($200,000 \text{ cm}^2\text{V}^{-1}\text{S}^{-1}$), excellent transparency (-97.7%) and large surface area ($2600 \text{ m}^2/\text{g}$) [1–5]. Therefore, it has been intensively applied in electronic and optoelectronic devices [6–9]. However, the weak light absorption of rGO results in the poor photoelectrical performances, thereby limiting its application in photodetectors. Fortunately, the formation of composites can greatly improve or change the properties of materials [4, 5, 10]. So far, semiconductor nanocrystals, such as Zinc oxide (ZnO), Cadmium sulfide (CdS), Tungsten sulfide (WS_2), have been introduced into rGO to improve the optical and electronic properties [11–14].

ZnO is a semiconductor material with wide band gap of 3.37 eV and high excitation binding energy of 60 meV at room temperature, which makes it widely applied in the field of thermoelectric devices, bio-sensing, photodiodes and photoconductors in UV–visible spectral region, et al. [15–18]. Over the past decades, tremendous researches on photodetecting nanomaterials have revealed that the combination of long lifetime and short transit time of photogenerated electron–hole pairs can boost the photosensitivity [3]. Therefore, many researchers have tried to restrain the recombination of photogenerated electron–hole pairs and enhance charge transport by doping elements or forming composites with different bandgap materials and metal nanocrystals [3].

Due to these excellent optoelectronic properties of rGO and ZnO, rGO/ZnO nanocomposite is emerging as a new candidate material for high-performance photodetectors. However, because of the high surface-to-volume ratio, ZnO nanocrystals usually tend to aggregate onto the surface of rGO in the preparation process, which results in a higher recombination rate of photogenerated electronic-hole pairs [5]. Researchers have utilized surfactants (e.g.,

✉ Xiao Zhu
xzl412@126.com

✉ Shenglin Jiang
lhshust@163.com

¹ School of Optical and Electronic Information, Huazhong University of Science and Technology, 1037 Luoyu Road, Wuhan 430074, People's Republic of China

polyvinyl pyrrolidone (PVP), poly (acrylic acid) (PAA)) to avoid the agglomeration of zinc nanocrystals on the rGO surface; but, these dispersants are not then easy to remove and sometimes these dispersants are even toxic [19]. To solve this problem, we utilize the negatively charged surface of graphene oxide (GO) to absorb positively charged Zn^{2+} ions, avoiding the use of surfactants. However, the oxygen-containing groups (e.g., hydroxyl, carboxyl and epoxy groups) on graphene oxide makes it to be electrically insulating. Thus, it is necessary to reduce GO for facilitating the carrier transport more efficiently. Thermal reduction, as one of the common methods for reducing GO, has been performed at high temperature (400–1000 °C) [11, 20, 21]. But, the high temperature process have severe demand on the equipment and environment, such as vacuum or inert gas environment. In order to reduce GO, the GO/ZnO nanocomposite has to be placed in Ar gas protective atmosphere during thermally reduction process at 700 °C, unfortunately, this high temperature process caused the carbon doped in ZnO nanoparticles and deteriorated the photoelectrical properties of nanocomposite [11]. Moreover, the high temperature process is incompatible with flexible substrates electronics or device fabrication techniques. Therefore, a low processing temperature is highly desirable for reducing GO in the fabrication of the rGO/ZnO nanocomposite photodetector.

In this paper, a facile low temperature annealing process (<170 °C) combined with a solvothermal method is used to prepare rGO/ZnO nanocomposite photodetectors for the first time. In our strategy, there is no any surfactant used. Pure ZnO and rGO/ZnO nanocomposites are annealed at various low-temperatures. The results of Fourier Transform InfraRed and Raman spectra indicate that the graphene oxide in the nanocomposite has been reduced to rGO via a low-temperature annealing process. The photoresponse properties of rGO/ZnO nanocomposites are also significantly improved due to the enhanced ability of carrier transport of rGO. Hence, the low-temperature annealing process is a simple and low-cost technique to fabricate rGO/ZnO nanocomposites for high performance UV photodetector.

2 Experimental procedure

2.1 Photodetector fabrication and test

The scheme of the rGO/ZnO nanocomposites preparation and UV photodetector fabrication were shown in Fig. 1.

The nanocomposites were prepared by a solvothermal method according to literature methods [11, 22]. Graphene oxide (GO) was purchase from Hengqiu Graphene

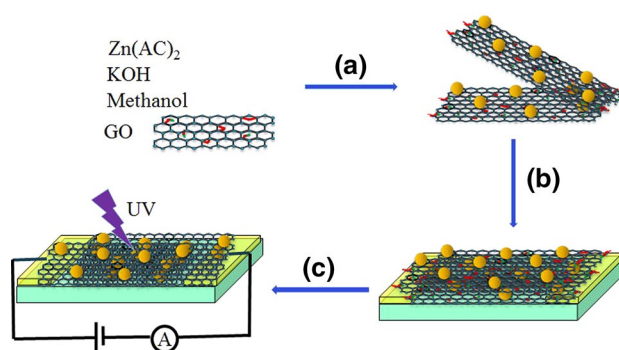


Fig. 1 Schematic diagrams of the preparation of rGO/ZnO nanocomposites and UV photodetector. (a) Synthesis of rGO/ZnO nanocomposites by solvothermal process, (b) Spin coating the nanocomposites on the Al_2O_3 substrates, (c) The nanocomposites were annealed at 130, 150 and 170 °C in the vacuum oven respectively

Technology (Suzhou) Co.Ltd. Zinc acetate ($\text{Zn}(\text{Ac})_2$, 4.46 mmol purity 99.99%) was added into a flask containing 42 mL of methanol and the solution was stirred for 15 min. Then 100 μL GO methanol solution (2 mg/mL) was added into $\text{Zn}(\text{Ac})_2$ methanol solution with vigorous stirring for 30 min to get a uniform suspension. Subsequently, the suspension was heated to 60 °C with vigorous stirring. Potassium hydroxide (KOH, purity 85%, 7.22 mmol,) was dissolved into 23 mL methanol as the stock solution that was dropped into the flask within 4–6 min. Then, the mixture was maintained at 60 °C for 2 h and 15 min with stirring. After the flask was cooled to room temperature and precipitated for 4 h, the upper fraction of the solution was removed. 50 mL methanol was added into the solution and stirred for 5 min. The upper fraction of the solution was removed again after 4 h. This process was repeated twice. Finally, the obtained products were dissolved in a mixed solvent of chloroform and methanol (6 mL, 2:1 by volume). For comparison, pure ZnO nanocrystal was prepared according to the same method above mentioned without adding GO.

Nanocrystal films and devices were fabricated on aluminum oxide substrates with Au electrodes (the distance was 300 μm and the length was 4 mm). The films were spin-coated with a speed of 2000 rpm for 30 s. Then the devices were respectively annealed at 130, 150, 170 °C in vacuum oven for 90 min.

2.2 Microstructure characterization

The crystallographic information of the obtained products was determined using an X-ray diffractometer. The morphology observation was conducted using a scanning electron microscope (SEM) and field emission transmission

electron microscope (FTEM) (Tecnai G2 F30). Fourier transform infrared (FTIR) analysis was performed on a Vertex 70 series spectrophotometer. Raman scattering of the nanocomposite was collected on a Renishaw in Via Raman microscope with an excitation laser of 532 nm. Absorption properties were investigated using a UV–vis spectrometer with detecting range from 325 to 700 nm. Photodetector device performance was measured by Agilent (B1500A, America) inside an optically and electrically sealed box. Lighting was generated through a functional generator (Agilent 33210A) controlled 365 nm light-emitting diode, and the power density irradiating to the device surface was around 690 μW/cm².

3 Results and discussion

Figure 2(a) shows the XRD patterns of GO, ZnO, GO/ZnO nanocomposites and the FTEM image of as-synthesized GO/ZnO nanocomposites. The XRD pattern of GO

displayed an intense and sharp diffraction at 2θ=10.8°, which was attributed to the (001) lattice plane corresponding to a d-spacing of 0.82 nm. This is consistent with the lamellar structure of GO. Both of pure ZnO and GO/ZnO nanocomposites showed diffraction peaks at 2θ=31.7°, 36.4°, 47.2°, 56.5°, 62.8°, 68.0° and 69.1°, which could be indexed to the (100), (101), (102), (110), (103), (112) and (201) lattice planes respectively of wurtzite structure ZnO [4, 23]. However, due to the crystallization of the products was not very well, the peak at 34.4° corresponding to (002) lattice plane was not observed. Furthermore, based on the XRD pattern, the average size of ZnO in GO/ZnO nanocomposites was estimated as 6.5 nm by using the Sherrer equation, which was well in accorded with the FTEM observation in the inset of Fig. 2(a). The XRD patterns of the annealed specimens were shown in Fig. 2(b). The major diffraction peaks of the annealed ZnO and rGO/ZnO nanocomposites were also indexed. However, the peaks from GO or rGO in the XRD pattern of the rGO/ZnO nanocomposites were not detected. This might be due to the inconsiderable amount of GO in nanocomposites samples. In addition, with the increase of annealing temperature, it could be discerned that the intensity of the peaks of rGO/ZnO nanocomposites significantly increased compared to pure ZnO. In fact, the rGO sheets could decrease the annealing temperature [20]. Thus, when the annealing temperature increases, rGO/ZnO nanocomposites had better crystallinity than pure ZnO because of the presence of GO. Figure 3 shows the SEM image of rGO/ZnO annealed at 150 °C. It was obvious that the rGO/ZnO films were uniform. The marked areas showed relatively obvious granular sensation.

The efficient reduction of GO to rGO after low-temperature annealing process was verified in the FTIR and

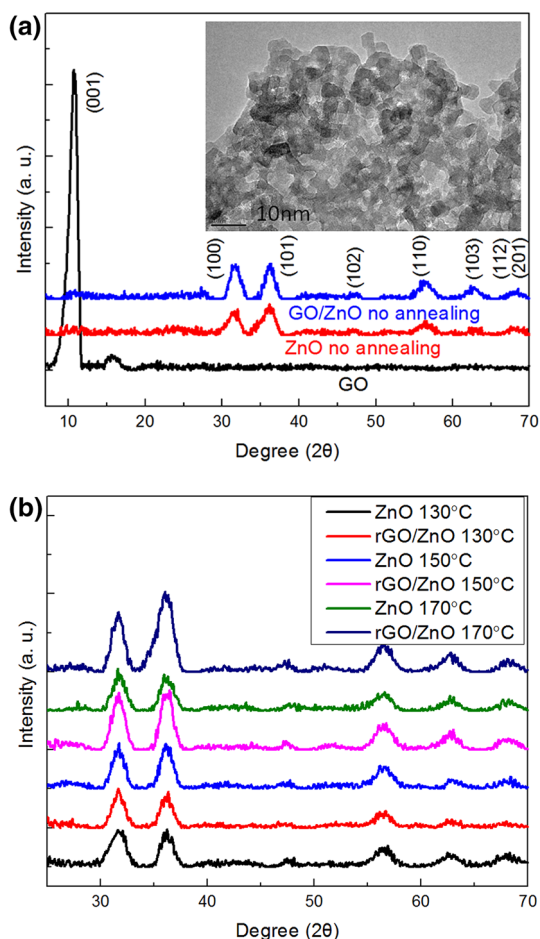


Fig. 2 XRD patterns of (a) GO, ZnO and GO/ZnO nanocomposites and (b) ZnO and rGO/ZnO nanocomposites annealed at various temperatures. The inset shows the FTEM image of GO/ZnO nanocrystals

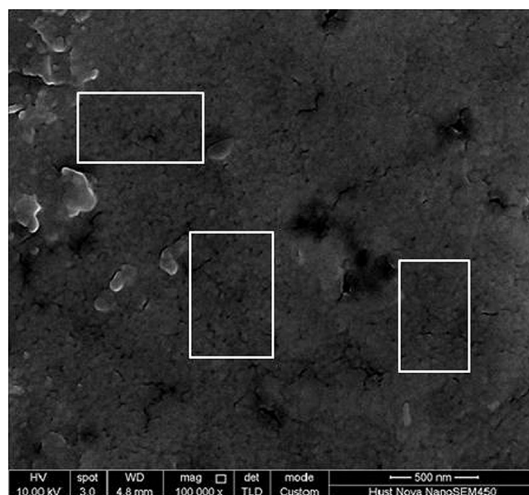


Fig. 3 SEM image of the rGO/ZnO annealed at 150 °C

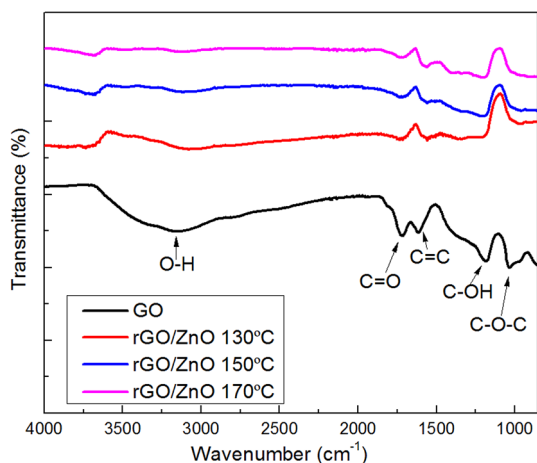


Fig. 4 FTIR spectra of GO and rGO/ZnO nanocomposites annealed at various temperatures

Raman spectra. Figure 4 shows the FTIR spectra of pristine GO and rGO/ZnO nanocomposites annealed at 130, 150 and 170 °C respectively. In the FTIR spectra, the broad peak centered at 3151 cm^{-1} was attributed to the O–H stretching vibration, and the peaks at 1716, 1614, 1183 and 1033 cm^{-1} were assigned to the vibration of C=O, the stretching vibration of C=C, the vibration of C–OH, the stretching vibration of C–O groups, respectively [19, 20]. It could be seen from the spectra that after the low-temperature annealing, the intensities of all bands related to the oxygen-containing functional groups were depressed or nearly vanished. This means that these oxygen-containing functional groups are removed in the low-temperature annealing process [20].

The Raman spectra of pristine GO and rGO/ZnO nanocomposites annealed at 130, 150 and 170 °C respectively

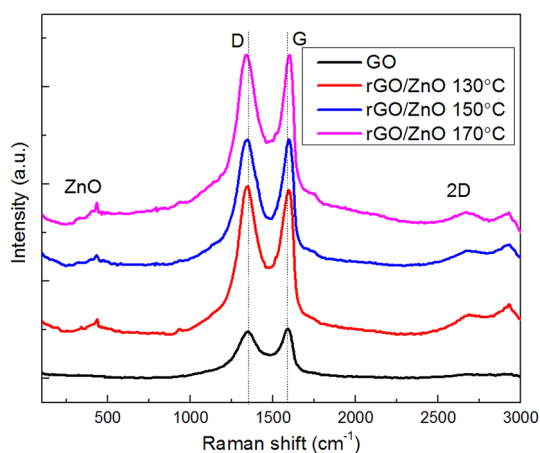


Fig. 5 Raman spectra of GO and rGO/ZnO nanocomposites annealed at various temperatures

were shown in Fig. 5. For the pristine GO, the *D* and *G* bands were centered at approximately 1348 and 1590 cm^{-1} , respectively. The *G* band is attributed to the in-plane bond stretching of the C–C sp^2 bond, and the *D* band is connected with the various disorders and defects, such as vacancy-like defects and sp^3 defects [5, 24]. After annealing rGO/ZnO nanocomposites at 130, 150 and 170 °C, the *D* peak showed a measurable shift to 1345, 1343 and 1337 respectively. This indicated that the graphene oxide in the nanocomposites samples have been reduced by the low-temperature annealing [5]. However, the *G* peak of the nanocomposites samples displayed a shift to 1593, 1596 and 1599 cm^{-1} respectively with the increasing of annealing temperature, which could be attributed to the chemical interaction between ZnO and graphene [23, 25]. Moreover, the 2*D* peak appeared at approximately 2673 cm^{-1} , which was known as a key sign of graphene sheets [26]. Furthermore, the peak at approximately 2924 cm^{-1} was due to the combination of the *D* and *D'* bands (*D*+*D'*) [5]. The intensity ratio of *D* to *G* band (I_D/I_G) in pristine GO was 0.937, while that for rGO/ZnO nanocomposites annealed at 130, 150, 170 °C were 1.0, 0.984, 0.962 respectively. Compared with pristine GO, the I_D/I_G ratio of nanocomposites exhibited a slight increase, which could be due to the presence of more defects and the interaction between ZnO nanocrystal and graphene sheets. But the I_D/I_G ratio for rGO/ZnO nanocomposites decreased with the increasing of annealing temperature, which indicated that the average size of the sp^2 domain increased upon the reduction of GO to rGO [4]. In addition to the rGO peaks, the Raman spectra of the rGO/ZnO nanocomposites showed a peak at 437 cm^{-1} corresponding to the E_2 (high) vibration mode of the Raman active mode, a characteristic peak for the wurtzite hexagonal phase of ZnO [11]. Therefore, after the low-temperature annealing, GO has been successfully reduced to rGO.

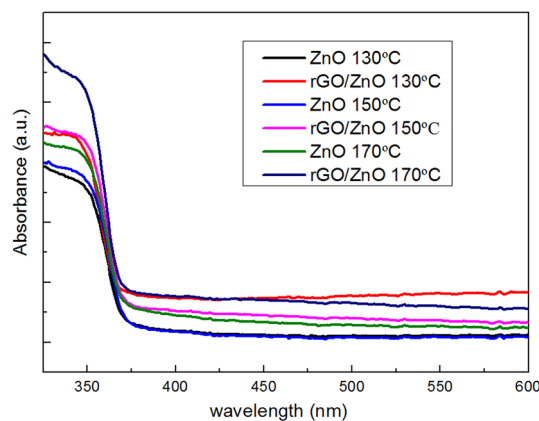


Fig. 6 UV–vis spectra of pure ZnO and rGO/ZnO nanocomposites annealed at various temperatures

The UV–vis absorption spectra of pure ZnO and rGO/ZnO nanocomposites annealed at various temperatures were shown in Fig. 6. As can be seen, because of the quantum confinement effect, the as-prepared pure ZnO and rGO/ZnO nanocomposites displayed a blue-shifted absorption peak at about 350 nm compared with that of bulk ZnO which has an absorption peak at 370 nm corresponding to a 3.35 eV bandgap at room temperature [27]. In addition, in the UV–vis absorption spectra, the introduction of rGO did not affect the peak positions of the nanocomposites. However, the absorption rate of rGO/ZnO nanocomposites increased compared with that of pure ZnO. This may be that there is an increase in surface electric charge of ZnO in the nanocomposites on account of introducing reduced graphene oxide, which may modify electron–hole pair formation during irradiation [4].

To investigate the effect of low-temperature annealing on the UV-light responsive behavior of rGO/ZnO detectors, time-resolved photoresponse test were conducted with a fixed bias of 10 V. Figure 7 shows the photocurrent response of ZnO and rGO/ZnO nanocomposites annealed at various temperatures. It can be seen that the generated photocurrents were dramatically enhanced after the introduction of rGO annealed at low-temperature. When the annealing temperature was 130 °C, the photocurrent of the rGO/ZnO nanocomposite was 721 nA, which was much higher than that of the pure ZnO with 192 nA. Similarly, when the annealing temperature was 150 and 170 °C, the photocurrents increased from 452 nA to 1.18 μ A and from 607 to 2.71 μ A respectively because of the existence of rGO. When the annealing temperature was 170 °C, the photocurrent of rGO/ZnO was about 4.5 times larger than pure ZnO, and the corresponding detectivity reached to 6.39×10^{10} Jones. This is probably that the photogenerated electrons on the conduction band of ZnO are trapped by the rGO, which prevents the recombination of photogenerated electron–holes pairs, and simultaneously rGO serves as the carrier collector transporting the carriers to the electrodes efficiently [20]. Moreover, the higher the annealing temperature was, the larger the photocurrent of rGO/ZnO nanocomposites was, which also can be observed in Fig. 8 (b). This was due to that the reduction degree of rGO was improved when the annealing temperature increased, which had been verified by FTIR and Raman spectra. The high reduction degree of rGO was contributed to the separation and transfer of carriers. Thus, when the annealing temperature was 170 °C, the photocurrent of rGO/ZnO nanocomposites remarkably enhanced compared with pure ZnO, as shown in Fig. 7 (c). In addition, the response time was about 5.26 s and the recovery time was around 11.4 s for

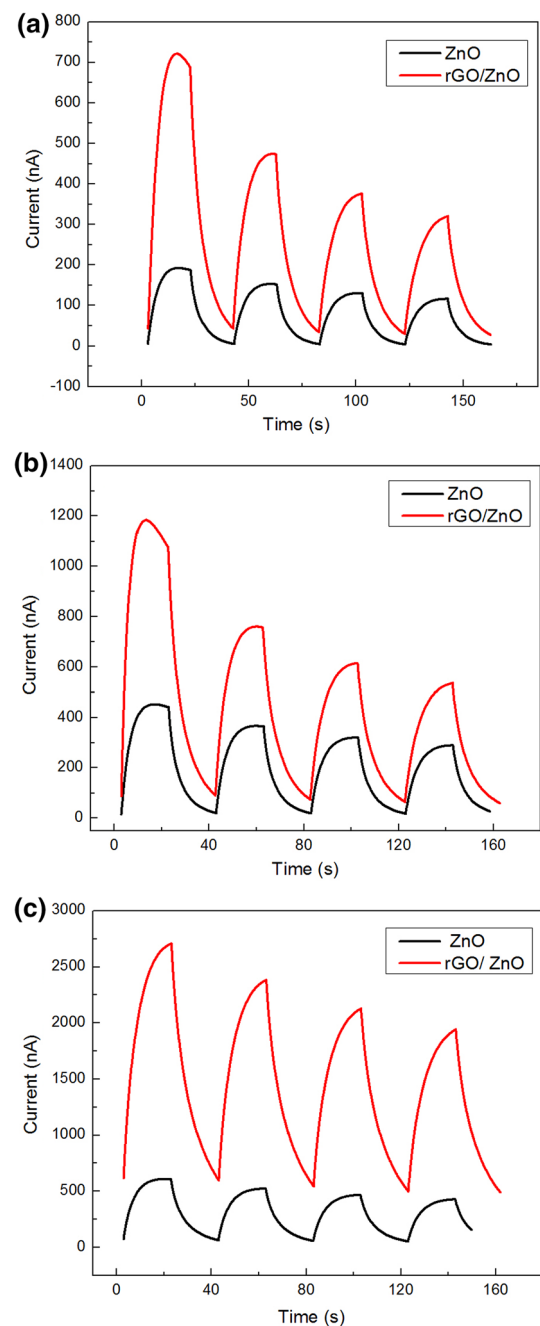


Fig. 7 The photocurrent response of pure ZnO and rGO/ZnO nanocomposites with different annealing temperature (a) 130 °C, (b) 150 °C, (c) 170 °C

rGO/ZnO photodetector when the annealing temperature was 150 °C, which was much faster than many other ZnO nanostructures exhibited a response time range from decades of seconds to a few minutes [28]. Figure 8 showed the effect of annealing temperature on the photoresponse

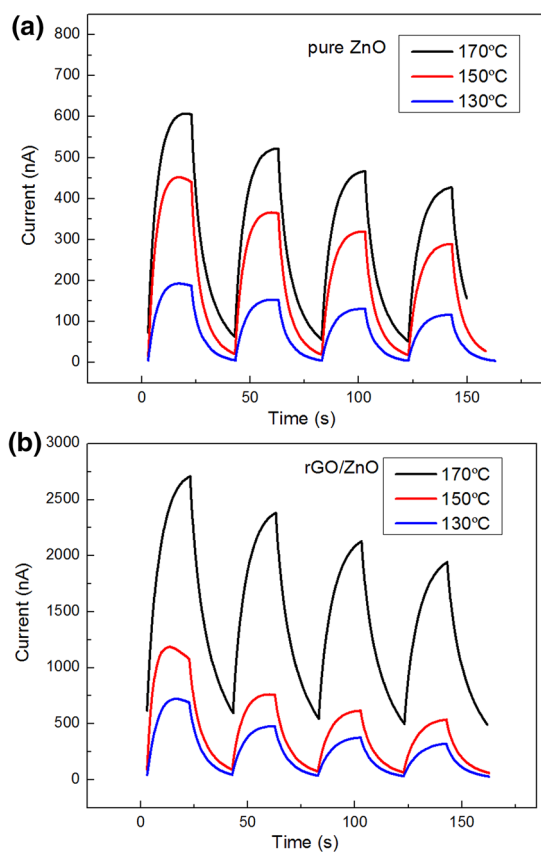


Fig. 8 The effect of annealing temperature on the photocurrent response (a) pure ZnO and (b) rGO/ZnO nanocomposites

of pure ZnO and rGO/ZnO nanocomposites. It should be noted that the increase of annealing temperature also gave rise to the enhancement of photocurrent in the pure ZnO samples. This may be due to a certain degree of particle sintering [27]. However, the improvement effect of photocurrent was more prominent in the rGO/ZnO samples. This indicated that the improvement of photocurrent in rGO/

ZnO nanocomposite was the result of combined effects of the reduced graphene oxide and further sintered ZnO by low-temperature annealing. It's worth noting that although the photoresponsivity of rGO/ZnO being poorer than that of other UV photodetectors, the photocurrent significantly increases and the response and recovery time are fast by utilizing this simple method, and the results are summarized in Table 1. We believe that the low-temperature annealing to reduce GO is a simple and low-cost method to improve the photoelectronic properties of rGO/ZnO nanocomposites.

4 Conclusion

In summary, rGO/ZnO nanocomposite have been successfully prepared by cost-effective solvothermal method and low-temperature annealing process ($<170^{\circ}\text{C}$) for photodetector application. Through the low-temperature annealing process, graphene oxide in the GO/ZnO nanocomposites have been reduced effectively and the reduction degree of graphene oxide became higher with the increasing of annealing temperature. On the other hand, the introduction of rGO in rGO/ZnO nanocomposite boosted the light absorption at the ultraviolet light region. Therefore, the photocurrent of rGO/ZnO samples was obviously improved, which was about 4.5 time than that of pure ZnO samples, and the corresponding detectivity reached 6.39×10^{10} Jones. In addition, for the rGO/ZnO nanocomposite, the photocurrents were also improved with the increasing of annealing temperature due to the enhancement of the reduction degree. The excellent properties of rGO/ZnO nanocomposite indicates that the low-temperature annealing process provides a facile and low-cost approach to prepare high-performance nanocomposites photodetectors, which can be extended to other material systems for practical application.

Table 1 The performance comparison of different ZnO nanocomposites based photodetectors

Photodetector	Bias (V)	I_{dark}	I_{ph}	R (A/W)	t_{rise}	t_{decay}	Switch ratio	Light (nm)	$L_{\text{spacing gap}}$	Ref.
ZnO QDs-G	2	600 nA	1.2 μA	–	0.29 s	0.29	–	365	–	[29]
ZnO-G	–	–	–	1.32	30.8 s	57.2 s	2.28	368	1 mm	[26]
ZnO hollow-sphere	5	50 nA	2.6 μA	13.5	467 μs	940 μs	–	350	30 μm	[30]
ZnO nanowire	3	1.87 μA	2.36 mA	–	19.6 s	2.5 s	–	365	–	[31]
ZnO NCs	10	157 μA	633 μA	54	20 s	142 s	–	390	300 μm	[32]
rGO/ZnO(150 $^{\circ}\text{C}$)	10	95.6 nA	1.18 μA	0.132	5.26 s	11.4 s	12.3	365	300 μm	This work

Acknowledgements The present study was supported by the National Nature Science Foundation of China (0204182087). We acknowledge the Analytical and Testing Center of Huazhong University of Science and Technology for characterizations of our samples. We specially thank associate professor Liu Huan at Huazhong University of Science and Technology for providing the preparation conditions and equipments of nanocomposites materials. And we sincerely thank professor Tang Jiang at Huazhong University of Science and Technology to provide a semiconductor device analyzer for our testing.

References

- R.R. Nair, P. Blake, A.N. Grigorenko, K.S. Novoselov, T.J. Booth, T. Stauber, N.M.R. Peres, A.K. Geim, *Science* **320**, 1308 (2008)
- M.S. Poorali, M.M. Bagheri-Mohagheghi, *J. Mater. Sci. Mater. El.* **27**, 10411 (2016)
- X.B. Liu, H.J. Du, X.W. Sun, *RSC Adv.* **4**, 5136 (2014)
- M.K. Kavitha, H. John, P. Gopinath, R. Philip, *J. Mater. Chem. C* **1**, 3669 (2013)
- M. Sookhastian, Y.M. Amin, R. Zakaria, W.J. Basirun, M.R. Mahmoudian, B. Nasiri-Tabrizi, S. Baradaran, M. Azarang, *J. Alloy. Comp.* **632**, 201 (2015)
- D.Z. Zhang, H.Y. Chang, P. Li, R.H. Liu, *J. Mater. Sci. Mater. El.* **27**, 3723 (2016)
- Q.L. Bao, K.P. Loh, *Graphene photonics. ACS Nano* **6**, 3677 (2012)
- H. Abdullah, N.A. Atiqah, A. Omar, I. Asshaari, S. Mahalingam, Z. Razali, S. Shaari, J. S. Mandeep, H. Misran, *J. Mater. Sci. Mater. El.* **26**, 2263 (2015)
- B. Chitara, S.B. Krupanidhi, C.N.R. Rao, *Appl. Phys. Lett.* **99**, 113114 (2011)
- H.B. Zhang, C. Groh, Q. Zhang, W. Jo, K.G. Webber, J. Rödel, *Adv. Electron. Mater* **1**, 1500018 (2015)
- Z.Y. Zhan, L.X. Zheng, Y.Z. Pan, G.Z. Sun, L. Li, *J. Mater. Chem* **22**, 2589 (2012)
- D.L. Shao, M.P. Yu, H.T. Sun, T. Hu, J. Lian, S. Sawyer, *Nanoscale* **5**, 3664 (2013)
- J.Q. Yu, J. Jin, B. Cheng, M. Jaroniec, *J. Mater. Chem. A* **2**, 3407 (2014)
- S. Ratha, A.J. Simbeck, D.J. Late, S.K. Nayak, C.S. Rout, *Appl. Phys. Lett.* **105**, 243502 (2014)
- D.P. Norton, Y.W. Heo, M.P. Ivill, K. Ip, S.J. Pearton, M.F. Chisholm, T. Steiner, *Mater. Today* **7**, 34 (2004)
- M. Norouzi, M. Kolaoudoz, P. Ebrahimi, M. Ganjian, R. Soleimanzadeh, K. Narimani, H. Radamson, *Thin Solid Films* **619**, 41 (2016)
- B.D. Boruah, A. Mukherjee, S. Sridhar, A. Misra, *ACS Appl. Mater. Inter.* **7**, 10606 (2015)
- Z.H. He, X.Q. Meng, *J. Mater. Sci. Mater. El.* **24**, 3365 (2013)
- L.H. Yu, H. Ruan, Y. Zheng, D.Z. Li, *Nanotechnology* **24**, 375601 (2013)
- M. Azarang, A. Shuhaini, R. Yousefi, M. Sookhastian, *J. Appl. Phys.* **116**, 084307 (2014)
- Y.L. Zhang, L. Guo, H. Xia, Q-D. Chen, J. Feng, H-B. Sun, *Adv. Optical Mater.* **2**, 10 (2014)
- B.Q. Sun, H. Siringhaus, *Nano Lett.* **5**, 2408 (2005)
- K. Anand, O. Singh, R.C. Singh, *Appl. Phys. A* **116**, 1141 (2014)
- H. Liu, Q. Sun, J. Xing, Z.Y. Zheng, Z.L. Zhang, Z.Q. Lu, K. Zhao, *ACS Appl. Mater. Inter.* **7**, 6645 (2015)
- T.G. Xu, L.W. Zhang, H.Y. Cheng, Y.F. Zhu, *Appl. Catal. B- Environ.* **101**, 382 (2011)
- S. Safa, R. Sarraf-Mamoory, R. Azimirad, *J. Sol-Gel. Sci. Techn.* **74**, 499 (2015)
- Y.Z. Jin, J.P. Wang, B.Q. Sun, J.C. Blakesley, N.C. Greenham, *Nano Lett.* **8**, 1649 (2008)
- Z.X. Wang, X.Y. Zhan, Y.J. Wang, S. Muhammad, Y. Huang, J. He, *Nanoscale* **4**, 2678 (2012)
- B.D. Boruah, A. Misra, *RSC Adv.* **5**, 90838 (2015)
- M. Chen, L.F. Hu, J.X. Xu, M.Y. Liao, L.M. Wu, X.S. Fang, *Small* **7**, 2449 (2011)
- L. Ren, T.T. Tian, Y.Z. Li, J.G. Huang, X.J. Zhao, *ACS Appl. Mater. Inter.* **5**, 5861 (2013)
- X.L. Tong, X.Z. Xia, Q.X. Li, *Chinese Phys. B* **24**, 067306 (2015)